# Quantum-walk transport properties on graphene structures

Hamza Bougroura,[1,2,3,*] Habib Aissaoui,[1] Nicholas Chancellor,[3] and Viv Kendon[3,†]
[1]*Laboratoire de Physique Mathematique et Subatomique (LPMS), University of Constantine 1, Algeria*
[2]*Department of Physics, Faculty of Exact Science, University of Tebessa, Algeria*
[3]*Department of Physics, Durham University, South Road, Durham DH1 3LE, United Kingdom*
(Received 19 September 2016; published 23 December 2016)

We present numerical studies of quantum walks on $C_{60}$ and related graphene structures to investigate their transport properties. Also known as a *honeycomb lattice*, the lattice formed by carbon atoms in the graphene phase can be rolled up to form nanotubes of various dimensions. Graphene nanotubes have many important applications, some of which rely on their unusual electrical conductivity and related properties. Quantum walks on graphs provide an abstract setting in which to study such transport properties independent of the other chemical and physical properties of a physical substance. They can thus be used to further the understanding of mechanisms behind such properties. We find that nanotube structures are significantly more efficient in transporting a quantum walk than cycles of equivalent size, provided the symmetry of the structure is respected in how they are used. We find faster transport on zigzag nanotubes compared to armchair nanotubes, which is unexpected given that for the actual materials the armchair nanotube is metallic, while the zigzag is semiconducting.

DOI: 10.1103/PhysRevA.94.062331

## I. INTRODUCTION

Quantum versions of random walks have been extensively studied for the past three decades, leading to a range of applications. In this paper, we focus on their transport properties. Their potentially exponential quantum speedup over equivalent classical random-walk transport was first proved in an algorithmic setting by Kempe [1,2] on a hypercubic graph, followed by Childs *et al.* [3] on a specially chosen "glued trees" graph. In a physical setting, quantum transport on spin chains [4] is isomorphic to continuous-time quantum walks. This led to intensive study of how to optimize quantum state transfer over short chains, as reviewed by Kay [5,6], with applications such as quantum wires to connect components in quantum devices for communication and computation. Quantum walks can also reproduce the phenomenon of Anderson localization [7–9], highlighting the importance of controlling the quantum-walk parameters to achieve efficient transport. Studies by Krovi and Brun [10,11] expose the role of symmetry in the underlying graph structures in quantum-walk transport.

Noting the importance of graphene and related substances as materials with many interesting electrical properties [12–17], in this paper we apply quantum versions of random walks to study quantum transport properties on various structures based on $C_{60}$ and graphene lattices. The variation in conductivity of graphene is exploited in diverse application [18–22]. Recently, continuous-time quantum walks on graphene lattices have been studied by Foulger *et al.* [23] to implement a quantum-walk search algorithm and apply this to communications between selected nodes on the lattice. The lattice is also called "honeycomb" and other studies of quantum walks on this type of graph can be found in [24–26].

Analytical solutions for quantum walks on graph structures are challenging. Even the simplest cases of the cycle [27], hypercube [28], and Cartesian lattices [29–31] require significant mathematical effort. For perfect state transfer on small graphs, where the quantum state of the walker is exactly reproduced at the target node, analytical results are known for a few special cases, reviewed by Kendon and Tamon [32]. This is also because perfect state transfer is hard to achieve in general, and for many applications it is sufficient to obtain fast probabilistic transfer. Analytical solutions usually require a homogeneous graph structure, either finite or infinite, or parameter tweaking for each situation [6]. There are techniques to compose compatible small graph structures into larger ones [33] for which the analytical solutions can also be combined, but there are limitations to this method. For studies on more general structures, numerical simulation is the best option, allowing the range of structures to be extended to be more practically relevant. It is also generally the case that discrete-time and continuous-time quantum walks give similar results on the same graphs, and their equivalence has been shown analytically for the line [34] using a method that can be expected to generalize for other homogeneous lattices. While the continuous-time walk can be more tractable analytically, for numerical simulation the unitary operators of the discrete-time walk are more convenient than the numerical integration required for the continuous-time walk. We therefore carried out our studies using the discrete-time quantum walk. Discrete, coined quantum walks can be implemented using atoms trapped in optical lattices, for example, and honeycomb lattices can be created this way. Internal degrees of freedom of the atoms then play the role of the quantum coin by coupling to the direction of motion of the atoms as the optical lattice is modulated [35–38].

The paper is organized as follows. In Sec. II, we define our model of a quantum walk and discuss its behavior on cycles. In Sec. III, we apply the quantum walks to $C_{60}$ and graphene nanotubes, focusing on the efficiency of transport between specified points on the structures. In Sec. IV, we summarize

*h_bougroura@hotmail.com
†viv.kendon@durham.ac.uk

 

our findings and discuss their applications and directions for future research.

## II. QUANTUM WALKS ON GRAPHS

We define a discrete-time, coined quantum walk on a regular, connected, undirected graph $G$ as follows. First we specify the graph on which the quantum walk takes place. For a graph $G$ with $n$ nodes, let $V$ be the set of nodes and $E$ be the set of edges connecting pairs of nodes. We label each node with a unique number $v \in \mathbb{Z}_n$, and identify the edges by the labels of the nodes they connect. Thus, for $u,v \in V$, we have $(u,v) \in E$ iff there is an edge $(u,v)$ connecting node $u$ to node $v$. Graph $G$ is undirected, i.e., $(u,v) \equiv (v,u)$, and connected, and there is at most one edge between any pair of nodes. The degree $d(v)$ of node $v \in V$ is the number of edges meeting at $v$. For a regular graph of degree $d$, we have $d(v) = d \ \forall v \in V$. In order to support the dynamics of the quantum walk, at each node $v \in V$ we label the ends of the edges at that node from $0 \ldots (d-1)$ in an arbitrary but fixed order. For $a,b \in \{0 \ldots (d-1)\}$, we define an edge label function,

$$e(u,a) = (v,b), \tag{1}$$

that returns the ordered pair of labels at the other end of the $a$th edge at node $u$, i.e., the $b$th edge at node $v$.

A discrete-time, coined quantum walk on a regular, connected, undirected graph $G$ has a discrete Hilbert space $H = H_G \times H_d$, where $H_G$ has dimension $n$ corresponding to the number of nodes, and $H_d$ has dimension $d$ corresponding to the number of edges $d$ meeting at each node. We choose a natural and convenient set of basis states, $|j,c\rangle \equiv |j\rangle \otimes |c\rangle$, with $j \in \mathbb{Z}_n$ and $c \in \mathbb{Z}_d$. A quantum walker can thus be thought of as a particle with an internal degree of freedom of dimension $d$ that is located on a node, or in superposition on nodes, of the graph. A general state $|\psi(t)\rangle$ of the quantum walker at time $t$ can be written as

$$|\psi(t)\rangle = \sum_{j \in V, c \in \mathbb{Z}_d} \alpha_{j,c}(t)|j,c\rangle, \tag{2}$$

where the coefficients $\alpha_{j,c}(t)$ are complex amplitudes normalized such that $\sum_{j,c} |\alpha_{j,c}(t)|^2 = 1$. The dynamics of the quantum walk are unitary in discrete-unit time intervals [39]. We utilize a flip-flop shift operator $S$. For the benefit of those readers who are unfamiliar with the action of this shift operator, we will explain its action in detail for clarity. The operator $S$ acts on both the coin state and position of the walker to move it between nodes that are connected by edges. It is defined by its action on the basis states,

$$S|u,a\rangle = |e(u,a)\rangle = |v,b\rangle, \tag{3}$$

making use of the edge label function defined in Eq. (1). We note that $e[e(u,a)] = (u,a)$, and hence $S \cdot S|u,a\rangle = |u,a\rangle$, confirming that $S$ is its own inverse, and therefore unitary. A coin operator $C$ acts only on the coin degrees of freedom. We are free to choose $C$ to be any unitary operation of dimension $d$. There are some natural choices for $C$ that we will introduce and discuss later. The role of the coin operator is equivalent to tossing the coin in a classical random walk: it rearranges the amplitudes for different coin states. A single step of the quantum walk consists of a coin operation followed by a shift, giving

$$|\psi(t+1)\rangle = S \cdot (\mathbb{1}_n \otimes C)|\psi(t)\rangle, \tag{4}$$

where $\mathbb{1}_n$ is the identity operation on the position space $H_n$ of the quantum walker. A quantum walk of $T$ steps from an initial state of $|\psi(0)\rangle$ can be written as

$$|\psi(T)\rangle = \big(S \cdot (\mathbb{1} \otimes C)\big)^T |\psi(0)\rangle. \tag{5}$$

The initial state has a significant impact on the subsequent quantum walk, unlike for a classical random walk, where the initial state is irrelevant to the long-time behavior. This is because the quantum walk is a deterministic, unitary dynamics. The range of choices for the initial state is large, and we are interested in transport properties that are not particularly sensitive to the choice of initial state. For the quantum walk on the line, for example, the spreading rate is linear, regardless of the initial state [29]. For the studies presented here, we used unbiased, symmetric initial states, either in terms of the coin states at a single node or an equal superposition of such states on a group of neighboring nodes.

To motivate our choices of coin operators, we first consider a quantum walk on one of the simplest small graph structures, i.e., the cycle. A cycle $C_n$ with $n$ nodes has a set of edges $\{(j,j+1)\}$, with $j \in \mathbb{Z}_n$ and addition modulo $n$, so that node $(n-1)$ is connected to node 0. The shift operator is thus

$$S_C = \sum_j (|j+1,0\rangle\langle j,1| + |j-1,1\rangle\langle j,0|), \tag{6}$$

where we have used a consistent labeling of the nodes and ends of the edges such that the label 1 is on the end of the edge that connects node $j$ to node $j+1$, and vice versa for label 0; see Fig. 1. This choice of labels is not necessary, but it does simplify the analysis, both numerical and analytical. The cycle has degree $d = 2$, so we need a two-dimensional coin operator. Ideally, we also want our coin operator to be unbiased so that no matter which direction the walker arrived from, it has an equal chance of leaving by either edge. We can achieve this by using the Hadamard operator

$$H = \frac{1}{\sqrt{2}} \begin{pmatrix} 1 & 1 \\ 1 & -1 \end{pmatrix}. \tag{7}$$

A symmetric form

$$H_i = \frac{1}{\sqrt{2}} \begin{pmatrix} 1 & i \\ i & 1 \end{pmatrix} \tag{8}$$

can also be used. In general, a phase factor of $\pi$ ($-1$ and $i \times i$ in the above, respectively) can be distributed in various equivalent ways, with corresponding cosmetic changes in the quantum walk [40].

The discrete-time quantum walk on the cycle was solved analytically by Aharonov *et al.* [27], and its properties are well studied. Of particular note for our purposes is its use in quantum state transfer. Using cycles of even-$n$ size, the quantum walk starts at one node with the aim of reaching the opposite node. First noted for $n = 4$ by Travaglione and Milburn [41], this can provide perfect state transfer for suitably chosen coin operators (not always the unbiased Hadamards) [42,43] and initial states. We used a corresponding size of $n$

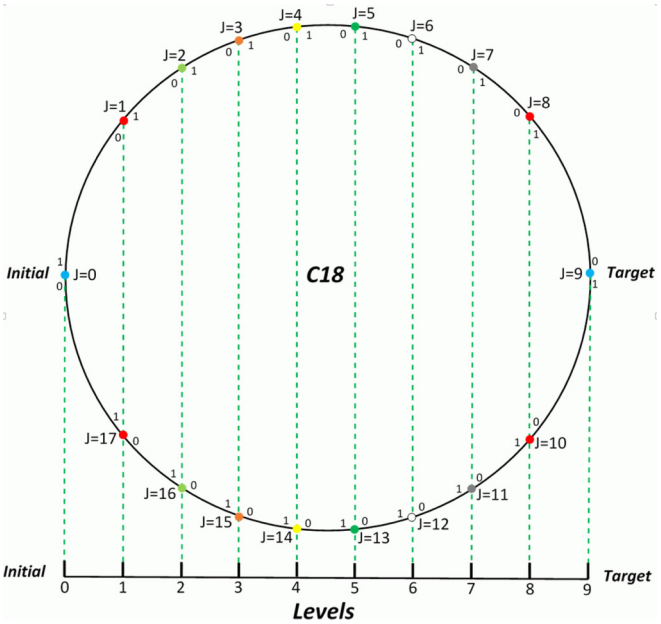


FIG. 1. A cycle $C_{18}$ with 18 nodes, showing a convenient set of node ($j$) and edge ($\{0,1\}$) labels as described in the text. The two opposite nodes are designated "Initial" and "Target," and the nodes between them are mapped in pairs (as colored, shaded grey) to a set of levels, so the progress towards the target node can be quantified.

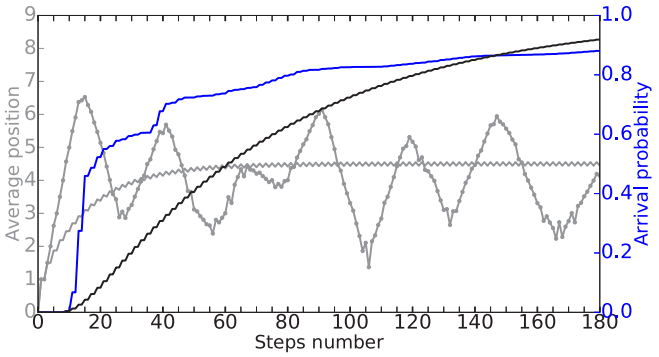


FIG. 2. 180 steps of a quantum walk on a cycle $C_{18}$ with 18 nodes mapped to 10 levels from start (0) to target node (9); see Fig. 1. Average position (gray, left axis) and arrival probability (blue, right axis) plotted against the number of time steps for coin operator $H$ (solid line, dark grey). A classical random walk using an unbiased two-sided coin (black) is shown for comparison.

cycle to provide a benchmark for evaluating the performance of quantum-walk transport on graphene structures.

### A. Numerical methods

Our numerical simulation code was written in PYTHON 3.5 using the NUMPY, SCIPY, and MATPLOTLIB packages [44–47]. Most of the simulations took no more than a few minutes each on standard desktop computers, so no special numerical optimization techniques were required. Figures of the $C_{60}$ and nanotube structures were drawn using VIRTUAL NANOLAB [48].

### B. Transport measures

There are many possible properties of quantum walks that can be calculated. For the smallest simulations, we visualized the probability distribution step by step to obtain a detailed picture of the behavior. We then calculated the average position over time, $\langle x \rangle$, where $x$ is the position mapped to levels as shown in Fig. 1,

$$\langle x \rangle = \sum_{c,j} x(j) |\alpha_{c,j}(t)|^2. \tag{9}$$

We also calculated the accumulated arrival probability $A(T)$. The accumulated arrival probability is equivalent to putting a "sink" at the target node and summing the probability of the walker being in the sink after each step of the quantum walk,

$$A(T) = \sum_{t=0}^{T} \sum_{c} |\alpha_{a,c}(t)|^2, \tag{10}$$

where $a$ is the target node, and $\alpha_{c,a}(t)$ is reset to zero before the next step of the quantum walk is applied. This is a nonunitary process with a practical operational interpretation. After each step of the quantum walk, the target node is measured to check for the presence of the walker. It will be found with probability $|\alpha_{c,a}(t)|^2$. With probability $1 - |\alpha_{c,a}(t)|^2$, the walker is somewhere else on the graph and the quantum walk continues to evolve, but without the amplitude on node $a$ because we just found out it is not there. Note that $A(T)$ is a monotonically increasing function of time because once the quantum walker has arrived at node $a$, it does not leave it. After comparing $\langle x \rangle$ with $A(T)$, we chose the latter as the clearest indicator of successful quantum transport.

With the sink at the target site, an analytical solution is even more challenging. For the cycle, a numerical comparison of average position and arrival probability is shown in Fig. 2, along with the equivalent quantities for a classical random walk, for comparison. For short times, the quantum walk arrives sooner, and the arrival probability approaches unity faster, than the classical random walk. For longer times, the curves cross and the classical random walk approaches unity faster. For very long times, both asymptote to unity (see the Appendix). In general, a quadratic speedup is expected for quantum walks on the cycle when compared with a classical random walk [49]. This is an asymptotic result for large cycles and does not apply directly to small cycles such as $C_{18}$. The short-time behavior, i.e., a steep rise in the arrival probability in the first 20 time steps, is the quantum speedup in this instance.

### C. Coin operators

There is another natural choice for the coin operator that models many realistic situations. As well as shifting to a connected node at each time step, the quantum walker may have a third choice, i.e., to stay at the current node. This can be achieved using a coin of dimension $c = d + 1$. Thus, for the cycle, this needs a coin of dimension three. We tested the walk on the cycle using a coin operator known as a Grover coin operator. The Grover coin operator can be defined for any

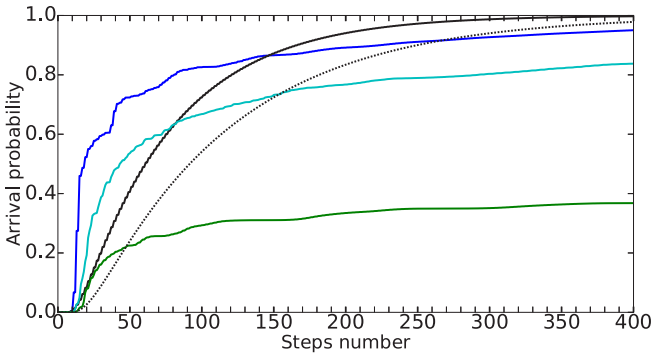


FIG. 3. A quantum walk of 400 steps on a cycle $C_{18}$ with 18 nodes mapped to 10 levels from start (0) to target node (9); see Fig. 1. Arrival probability plotted against the number of time steps for coin operators $H$ (blue, dark grey), $G_3$ (green, mid grey), and $F_3$ (turquoise, light grey). A classical random walk using an unbiased two-sided (black, solid line) and three-sided (black, dotted line) coin is shown for comparison.

dimension $d \geqslant 2$,

$$G_d = \frac{1}{d}\begin{pmatrix} 2-d & 2 & \cdots & 2 \\ 2 & 2-d & \cdots & 2 \\ \vdots & \vdots & \ddots & \vdots \\ 2 & 2 & \cdots & 2-d \end{pmatrix}. \tag{11}$$

For $d = 2$, it reduces to the Pauli $\sigma_x$ operator, which corresponds to steps in a single direction (completely biased). In three dimensions, it is

$$G_3 = \frac{1}{3}\begin{pmatrix} -1 & 2 & 2 \\ 2 & -1 & 2 \\ 2 & 2 & -1 \end{pmatrix}. \tag{12}$$

The Grover coin operator has the highest degree of symmetry possible in a unitary operator. The incoming direction is already special, but all other directions are treated exactly the same for both amplitude and phase of the outgoing state. The arrival probability for the quantum walk with a $G_3$ coin operator is shown in Fig. 3.

Another three-dimensional coin operator is the Fourier coin operator, which can also be defined for any dimension,

$$F_d = \frac{1}{\sqrt{d}}\begin{pmatrix} 1 & 1 & \cdots & 1 \\ 1 & \omega & \cdots & \omega^d \\ \vdots & \vdots & \ddots & \vdots \\ 1 & \omega^d & \cdots & \omega^{d\times d} \end{pmatrix}, \tag{13}$$

where $\omega = e^{2\pi i/d}$ is the complex $d$th root of unity. For $d = 2$, the Fourier coin operator reduces to the Hadamard coin operator in Eq. (7). The Fourier coin operator is unbiased for all dimensions, i.e., the walker is equally likely to leave by any available edge, regardless of which it arrived along. However, this comes at a cost of the relative phases being different for each direction to ensure the coin operator is unitary overall. Since the phase factors are what gives the quantum walk its advantage over the classical random walk, the Fourier coin operator can produce very different quantum-walk behaviors when compared with the Grover coin operator. The use of $F_3$ for a cycle with a "wait state" is also shown in Fig. 3. Out of all of these choices for coin operator, we can see that the Hadamard coin is the fastest: both $H$ and $G_3$ beat the classical random walk for short times, while $F_3$ only beats the classical three-sided coin for short times, and in fact never reaches the opposite side with certainty; see the Appendix.

## III. RESULTS

We now present our results for the transport properties of quantum walks on $C_{60}$ and various carbon nanotube structures. First, the different possible coin operators are compared on $C_{60}$. Then the role of symmetry in the structures themselves is investigated by using different combinations of starting nodes and target nodes. Finally, we studied nanotubes made from cylinders of graphene, both with capped ends and as loops, to explore how the width and length affect the overall transport efficiency.

### A. Comparison of coin operators on $C_{60}$

The graphene structures that are the focus of our work all have nodes with $d = 3$. Our first investigation was to compare several natural choices of coin operators to see how sensitive the transport properties are to different coin operations. Clearly, the $G_3$ coin of Eq. (12) is an obvious choice, along with $F_3$. We can also choose a $c = d + 1 = 4$ coin with a "wait state," with corresponding four-dimensional coin operators. We tested $G_4$ and $F_4$ and also a tensor product of two Hadamard coin operators, $H \otimes H$. In a similar manner as for the cycle, we chose an initial node on the $C_{60}$ structure and designated the opposite node the target node; see Fig. 4. The intermediate nodes are mapped to levels corresponding to the number of edges traversed on the shortest path from the initial node. Figure 5 shows a quantum walk on this $C_{60}$ structure from one node to the opposite node. From the graph,

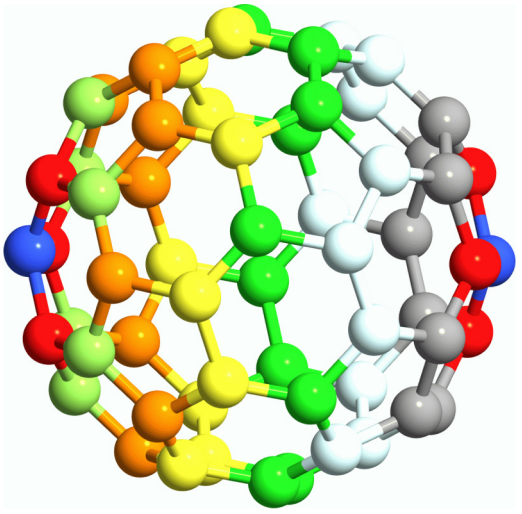

FIG. 4. A $C_{60}$ colored to indicate the levels from the initial node (blue, left, darkest grey): level 1 (red left, second darkest grey), level 2 (lime, fifth lightest grey), level 3 (orange , fourth darkest grey), level 4 (yellow, lightest grey), level 5 (green , sixth darkest grey), level 6 (white), level 7 (grey, third darkest grey), level 8 (red right, second darkest grey), level 9 (target, blue , darkest grey).

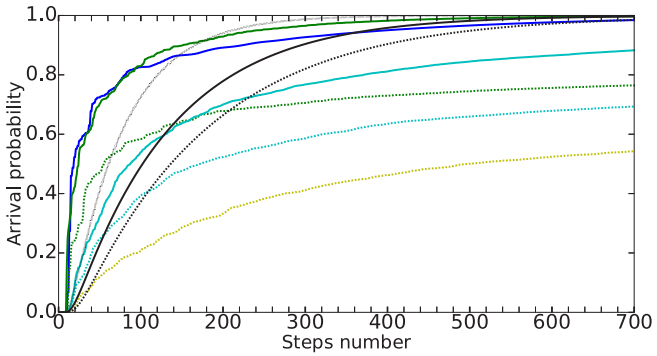


FIG. 5. A quantum walk of 700 steps on $C_{60}$ between single opposite nodes, mapped to 10 positions as in Fig. 4. Arrival probability plotted against the number of time steps for coin operators $G_3$ (green, solid line, mid grey), $G_4$ (green, dashed line, mid grey), $F_3$ (turquoise, solid line, light grey), $F_4$ (turquoise, dashed line, light grey), and $H \otimes H$ (yellow, dashed line, very light grey). A cycle $C_{18}$ is shown (blue, dark grey) along with classical random walks for a three-sided (black, solid line) and four-sided (black, dashed line) coin and the cycle (black, dotted line) for comparison.

we can see that the $G_3$ coin operator was consistently the best choice for transport properties, outperforming all the other walks even for long times. We have therefore focused on this coin operator for presenting the results in the following sections. We tested other coin operators on all structures and found their performance to be essentially the same in relation to $G_3$ as in Fig. 5. We also tested for more time steps (see Appendix) to confirm that all the $d = 3$ coins and the classical random walks do eventually arrive with unit probability, while the quantum walks with wait states do not.

### B. Role of symmetry in transport on $C_{60}$

We considered transport by quantum walk across $C_{60}$ with superposition initial and target states chosen to increase the symmetry between the initial and target nodes. Figure 6 shows two possible orientations with the initial and target nodes forming a face of the structure, as marked in blue. The transport from a single node to the diametrically opposite node shown in Figs. 4 and 5 has less symmetry than starting on a pentagonal face or a hexagonal face. It also has ten levels, rather than eight for the face-terminated orientations. A proper comparison of transport on these configurations must make allowance for this. We could give the ten-level systems a two-level head start. We can also compare with the corresponding cycles, $C_{14}$ and $C_{18}$, to provide a benchmark for the performance. Both give the same result, so we present the comparison with the cycles here. We find that the more symmetric initial states are more efficient, with the more symmetric hexagonal face slightly better than the pentagonal face. The details are shown in Fig. 7, to be compared with Fig. 5, using the line for the cycles $C_{14}$ and $C_{18}$, respectively, for calibration.

Figure 8 shows the structure end on, illustrating how the hexagonal face has higher symmetry compared with the pentagonal faces, which are inverted with respect to each other.

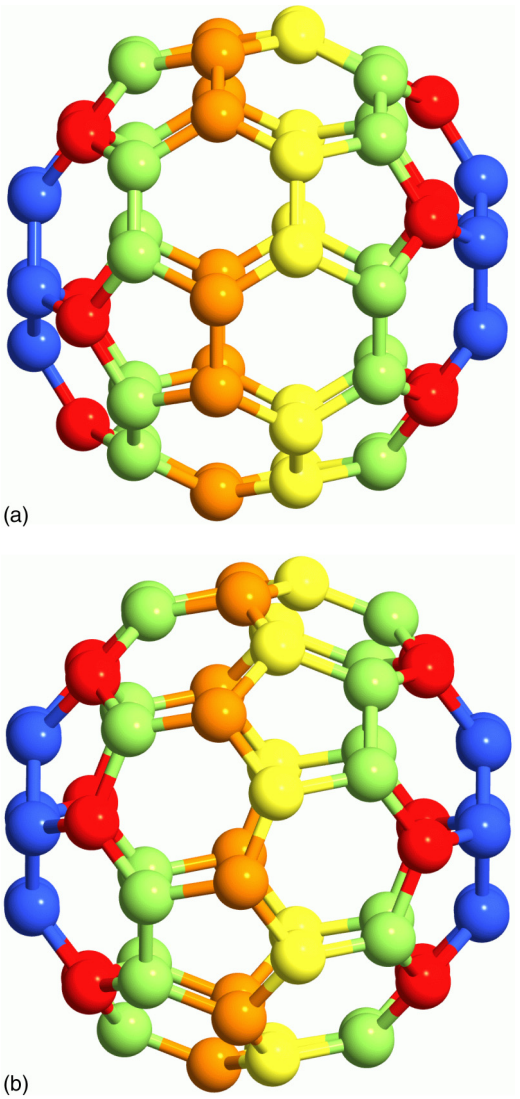


FIG. 6. $C_{60}$ with different initial positions (a) an equal superposition of all nodes of a pentagonal face, and (b) an equal superposition of all nodes of a hexagonal face. The nodes between the initial and target faces are colored (shaded grey) to indicate their grouping into eight levels.

### C. Transport on nanotube structures

We now turn to our studies of quantum-walk transport on graphene structures. There are two distinct ways to join up a sheet of graphene to form a tube, depending on whether the "zigzag" pattern runs round the tube or lengthways along the tube. The pattern orthogonal to the zigzag direction is known as "armchair." Thus we have zigzag nanotubes with the zigzag running around the tube, and armchair nanotubes with the zigzag running along the length of the tube. Both of these were tested and compared. There is a third way to join up graphene into nanotubes, where the zigzag runs obliquely. We did not test nanotubes of this type in this study because there are a rather large number of possibilities, all with less symmetry than the chosen configurations, and we have already demonstrated that symmetry significantly enhances transport on $C_{60}$.

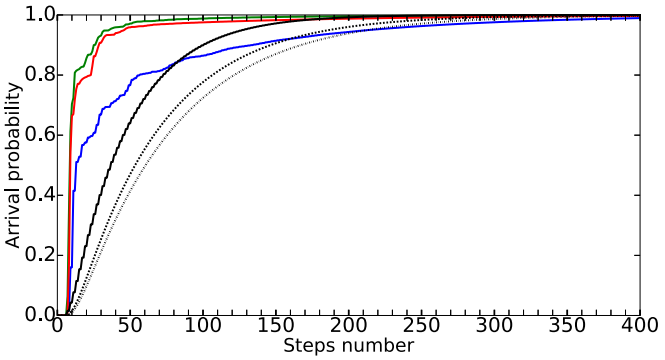


FIG. 7. A quantum walk of 400 steps on $C_{60}$ mapped to eight levels using the $G_3$ coin comparing different starting positions: hexagon (green, upper, darker mid grey) and pentagon (red, lower, lighter mid grey). A quantum walk with the $H$ coin on a cycle $C_{14}$ (blue, dark grey) is also shown. The corresponding classical random walks (black dashed, dotted, and solid lines, respectively) are shown for comparison.

In order to compare with the cycle, we joined the ends of the nanotubes to form a torus and studied the transport from one position on the ring to the opposite side; see Fig. 9. The distance from the start is projected onto a line segment in the same way as for the cycle shown in Fig. 1, so we can track the progress from the initial nodes to the target nodes.

The results for various diameters of zigzag and armchair nanotube are compared in Fig. 10, with the results for a cycle $C_{14}$ to provide a benchmark comparison. The first thing to note is that the diameter of the nanotubes does not affect the transport properties in this setting. Nanotubes of diameter six, ten, and 14 all gave identical results for the same length. Next we note that both forms of the nanotube are consistently better at transporting the quantum walk to the target nodes than the cycle $C_{14}$. The zigzag nanotube shows faster transport than the armchair nanotube, with both approaching unit probability eventually; see the Appendix.

To confirm the supremacy of the armchair nanotubes more generally, we also tested different lengths of nanotube; see Fig. 11. The pairs of zigzag (green) and armchair (red) plots can be seen to rise further apart for larger loops, indicating that the zigzag nanotube loops are providing faster transport

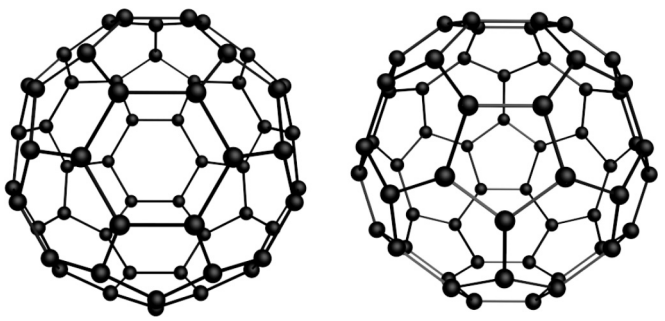

FIG. 8. $C_{60}$ viewed end on to illustrate how the hexagonal initial and target pair (left) are more symmetric than the pentagonal initial and target pair (right).

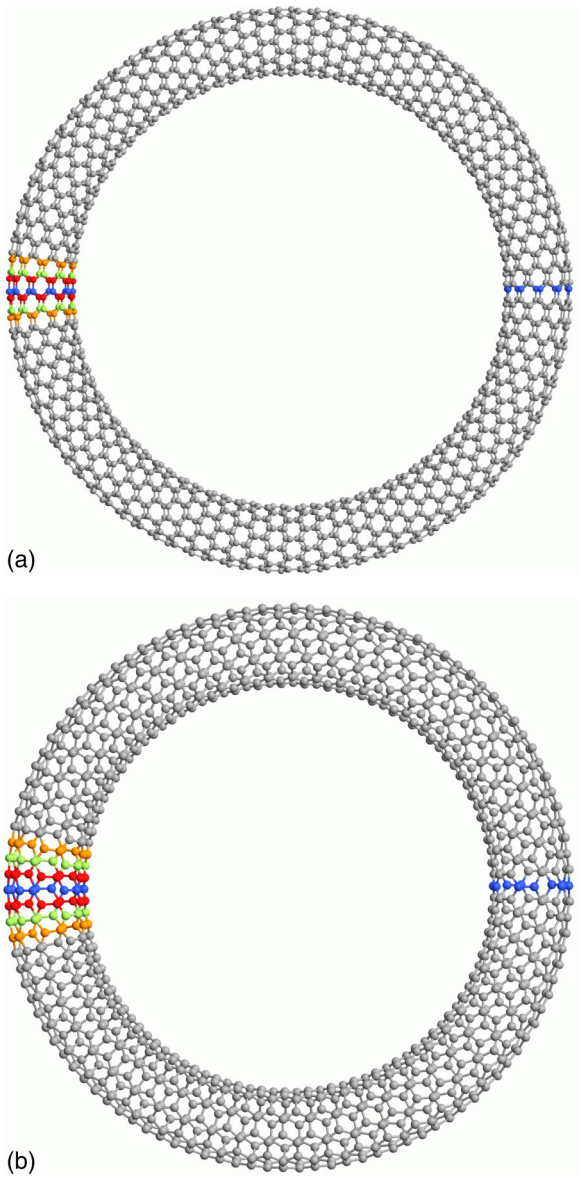


FIG. 9. (a) Zigzag carbon nanotube loop with 90 repeats forming 91 levels, and (b) armchair loop with 55 repeats forming 56 levels, from the sets of initial and target nodes marked in blue. A few of the nodes are colored (shaded) to indicate the mapping to levels; compare Fig. 1.

over the equivalent lengths. Both consistently outperform the cycles of equivalent lengths.

### D. Transport on capped nanotubes

Joining the nanotubes into loops like cycles puts a strain on the nanotubes and is not a natural form in which they occur. Bare ends of nanotubes can be irregular, which will not help with efficient coupling or transport. For nanotubes of matching diameter, a cap of half a $C_{60}$ structure can be attached to the ends. This is like having an elongated $C_{60}$ molecule, and the zigzag or armchair character determines whether the end of the cap is a pentagon or hexagon. An example with an armchair configuration that has pentagons at the ends is shown in Fig. 12.

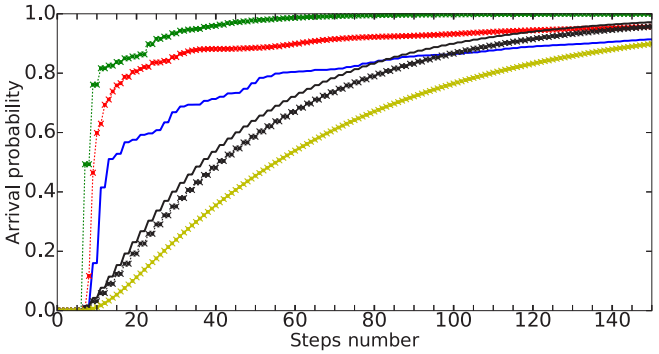


FIG. 10. A quantum walk of 150 steps on loops of zigzag (green, darker mid grey) and armchair (red, lighter mid grey) carbon nanotube with diameters of 6 (×), 10 (dashes), and 14 (circles), and length corresponding to eight levels. Cycle $C_{14}$ (blue, dark grey) is shown for comparison. Corresponding classical random walks shown in black (zigzag) and yellow (armchair, light grey), classical random walk on $C_{14}$ (black, solid line).

Results for quantum walks on these structures are shown in Fig. 13. The zigzag nanotubes give the fastest transport over short times, as can be seen more clearly for the longer lengths of nanotube. The armchair nanotubes providing the highest arrival probability at later times (the longer lengths were run for more steps to confirm this; not shown in Fig. 12). Both types of nanotubes outperform cycles of the same number of levels. A comparison between capped nanotubes and nanotube loops is shown in Fig. 14, revealing that the nanotube loops with the same number of levels are slightly better for short lengths, but worse for longer lengths, when the armchair capped nanotube approaches unit arrival probability fastest. This is likely due to the contribution from the caps reducing as a proportion of the total length for longer nanotubes. The long-time behavior of both is shown in the Appendix.

### E. Scaling of transport

Let us now consider the scaling of the transport rate on loops and capped nanotubes. To do this analysis, we examine the number of steps when the probability of arrival exceeds 50%, $N_{0.5}$ as a function of the number of levels in the structure. This captures short time behavior where Figs. 11–14 indicate that simple scaling might be obtained. This analysis allows us to differentiate between faster rates of transport on different structures (appearing as the slope of this quantity) and constant shifts in this quantity which may be caused by the formation of the wavefronts which propagate the walker. In addition to providing qualitative information, we perform linear fits to this data which provide quantitative measurements of the transport rates.

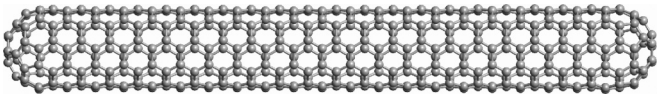

FIG. 12. An armchair nanotube with caps, with a pentagonal face at each apex. For a zigzag nanotube, the apices are hexagons (not shown). The level structure is as for the nanotube loops, but with only one round of carbon atoms per level.

Let us first consider the nanotube loops, for which the number of steps required for a 50% probability of arrival $N_{0.5}$ is plotted in Fig. 15. As we can see, the number of steps to reach 50% probability scales linearly with the number of levels, but does so at a different rate for different structures; therefore the difference in arrival time between armchair, zigzag, and loop geometries grows linearly with the number of levels. In fact by this metric, transport on a zigzag nanotube loop is almost twice as fast as on the cycle (see Table I for numbers extracted by numerical fitting).

We find similar results for the arrival time on capped nanotubes, as depicted in Fig. 16; however, we find that the difference in arrival times between zigzag and armchair is less dramatic. The data in Table I reveal that this is due to a combination of the fact that considering a capped rather than loop geometry makes transport on zigzag nanostructures slower, but makes the transport faster on armchair structures.

## IV. SUMMARY

We have demonstrated that transport for discrete-time quantum random walks is significantly faster on graphs corresponding to a variety of real-world nanostructures than it is on

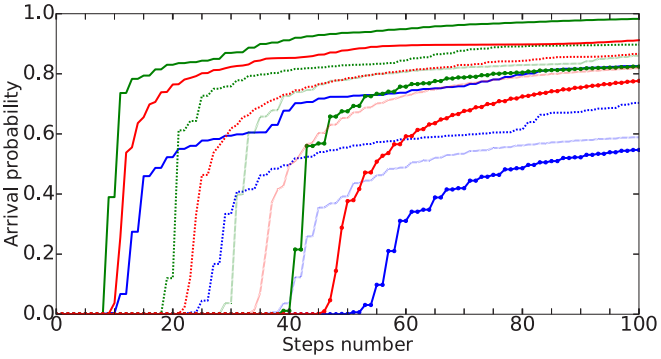


FIG. 11. A quantum walk on loops of carbon nanotube of length 10 (solid line), 20 (dashed line), 30 (dotted line), and 40 (circles, solid line) levels for zigzag (green, darker mid grey) and armchair (red, lighter mid grey). Cycles (blue, dark grey) of corresponding lengths are shown for comparison.

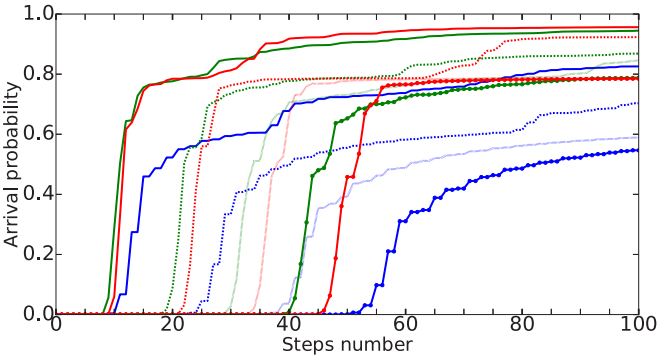


FIG. 13. A quantum walk on lengths of capped carbon nanotube: zigzag (green, darker mid grey), armchair (red, lighter mid grey) of lengths 10 (solid line), 20 (dashed line), 30 (dotted line), and 40 (circles, solid line). Cycles of corresponding lengths shown (blue, dark grey) shown for comparison.

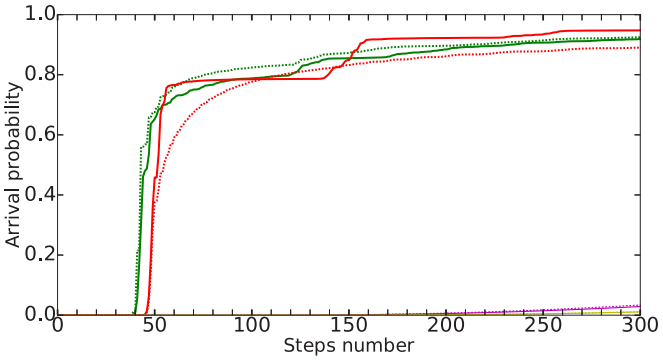


FIG. 14. A quantum walk of 300 steps on capped carbon nanotubes zigzag (green, solid line, darker mid grey) and armchair (red, solid line, lighter mid grey), compared with nanotube loops (dashed line).

simple cycles. In particular, we have demonstrated this for a $C_{60}$ fullerene graph and a variety of configurations of graphene nanotube structures, including nanotubes with fullerine caps. Our results consistently show that the nanostructures provide faster transport. Moreover, we demonstrate that in most cases, the walker eventually reaches the marked site with unit probability, thus showing that under many, but not all circumstances, these structures do not have the problem of infinite hitting times.

Transport across cycles is faster than on the line [6], hence we have also demonstrated that these structures provide faster transport than walks on a line. The fact that the coined discrete-time quantum-walk model exhibits faster transport than a simple line may be a discrete-time counterpart of the continuous-time effects which allow for ballistic transport on real-world carbon nanotubes [14–17].

The behavior on these materials can be traced back to the massless behavior of electrons at the Dirac point in the graphene band structure [13]. On the other hand, a discrete-time random walk does not carry with it an inherent notion of momentum or energy, so a band structure cannot be defined. In future work, it would be interesting to examine the possibility of a connection between the transport behavior we see and the band structure of these materials.

TABLE I. Values extracted from linear fit $y = mx + b$ for the data in Figs. 15 and 16 and coefficient of determination $r^2 \equiv 1 - \frac{\sum_i (y_i - f_i)^2}{\sum_i (y_i - \bar{y})^2}$, where $f_i$ are the data and $y$ is the fitting function, for each of the fits.

| Structure | $m$ | $b$ | $r^2$ |
|---|---|---|---|
| Cycle | 2.12 | −2.00 | 0.9996 |
| Loop: zigzag | 1.08 | 0.00 | 0.9986 |
| Loop: armchair | 1.43 | −2.00 | 0.9997 |
| Capped: zigzag | 1.20 | −1.50 | 0.9986 |
| Capped: armchair | 1.33 | −1.50 | 0.9996 |

We have also compared transport behavior between different nanostructures and have found that zigzag nanotubes exhibit faster transport than their armchair counterparts. In contrast, theoretical results for electrons in carbon nanotubes show that zigzag nanotubes behave as semiconductors, while armchair nanotubes behave as metals [16,17]. Therefore, in this respect, the relative transport efficiency between these structures for discrete-time random walks is qualitatively different from what is seen in electron transport. We further see that for capped nanotube structures, the arrival probability for a zigzag nanotube always approaches unity, while it does not for the armchair, again indicating better transport for the zigzag structures.

It would be interesting in future work to examine which one exhibits faster transport for continuous-time quantum walks with the same starting conditions that we used. On one hand, such walks would be subject to the band structure of the continuous material, but, on the other hand, they would be strongly out of equilibrium, unlike the cases typically examined in electronic transport calculations. Furthermore, it would be interesting to perform the same calculations as here, but with chiral nanotube structures, and compare the results

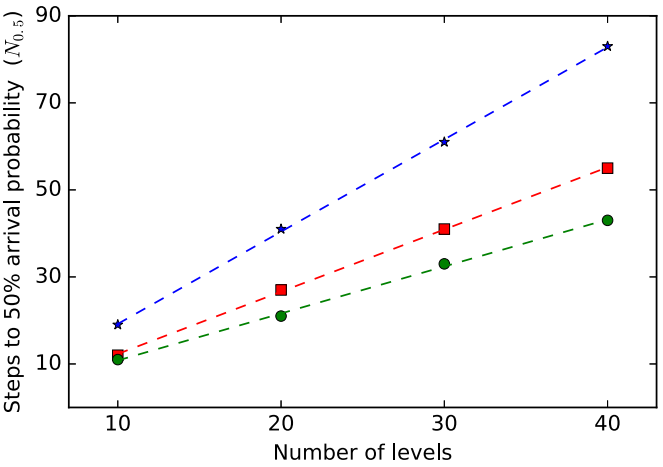


FIG. 15. Number of steps until 50% arrival probability vs number of levels for zigzag (green circles) and armchair (red squares) loop structures and the cycle (blue stars). Dashed lines are linear fits, the numbers extracted from these fits are summarized in Table I.

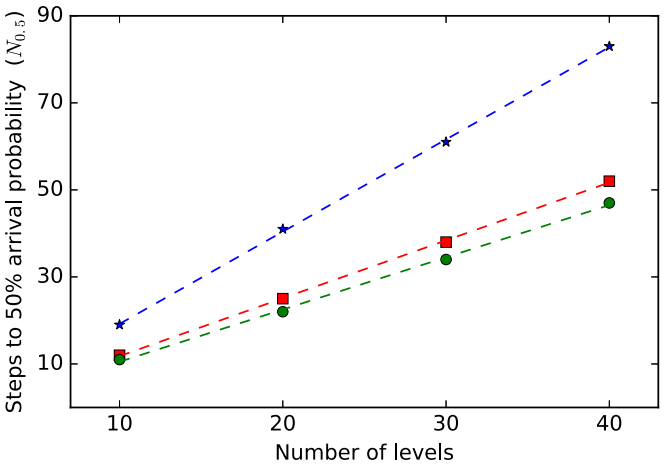


FIG. 16. Number of steps until 50% arrival probability vs number of levels for zigzag (green circles) and armchair (red squares) capped nanotube structures and the cycle (blue stars). Dashed lines are linear fits, the numbers extracted from these fits are summarized in Table I.

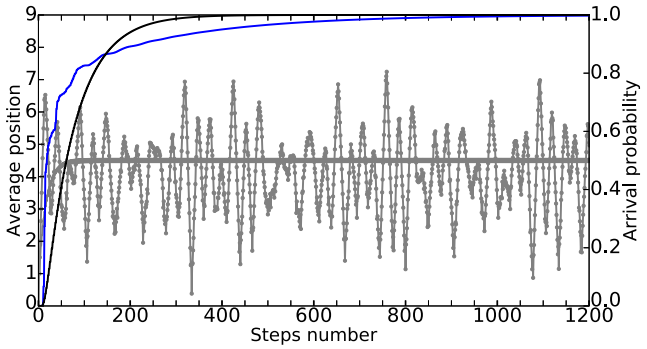


FIG. 17. Quantum and classical random walks on $C_{18}$ for 1200 steps showing that arrival times converge see right axis and corresponding black (classical walk) and blue (quantum walk, dark grey in print) lines to unity for both, while the oscillations about 4.5 for the average position continue indefinitely for the quantum walk, see left axis and corresponding (light) grey lines. Compare with Fig. 2.

with electronic behaviors to further investigate the relationship between electronic and quantum-walk properties.

## ACKNOWLEDGMENTS

H.B. is supported by the scholarship program of the Algerian Ministry of Higher Education and Scientific Research (Grant No. 459/PNE/ENS/GB/2015-2016), and Tebessa University. N.C. and V.K. are supported by the UK Engineering and Physical Sciences Research Council, Grant No. EP/L022303/1.

## APPENDIX: LONG-TIME BEHAVIOR OF QUANTUM WALKS

The long-term behavior of the quantum walks studied in this paper is presented here, in particular regarding whether the probability to arrive at the marked state approaches unity,

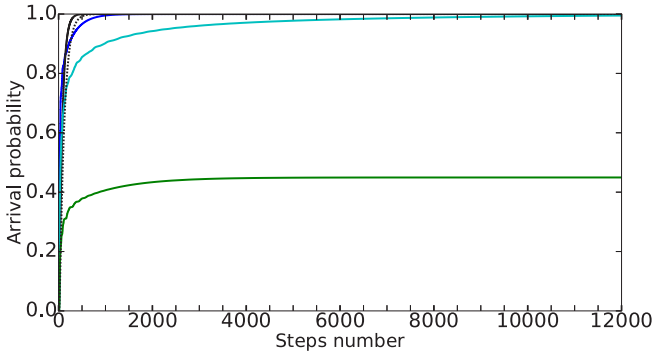


FIG. 18. Quantum and classical random walks on $C_{18}$ for 5000 steps showing the two-dimensional (2D) coins converge to unity, while the 3D coins do not in the quantum case, but do in the classical case. Here, 5000 steps of a quantum walk on a cycle $C_{18}$ with 18 nodes are mapped to 10 levels from start (0) to target node (9); see Fig. 1. Arrival probability plotted against the number of time steps for coin operators $H$ (blue), $G_3$ (green), and $F_3$ (turquoise). A classical random walk using an unbiased two-sided (black, solid line) and three-sided coin (black, dotted line) is shown for comparison.

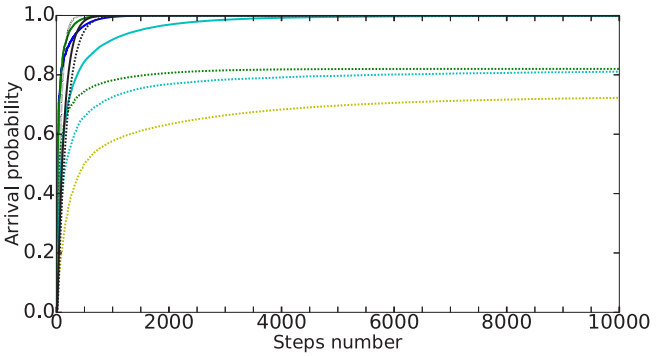


FIG. 19. A quantum walk of 10 000 steps on $C_{60}$ between single opposite nodes, mapped to 10 positions as in Fig. 4. Arrival probability plotted against the number of time steps for coin operators $G_3$ (green, solid line), $G_4$ (green, dashed line), $F_3$ (turquoise, solid line), $F_4$ (turquoise, dashed line), and $H \otimes H$ (yellow, dashed line). A cycle $C_{18}$ is shown (blue) along with classical random walks for a three-sided (black, solid) and four-sided (black, dashed) coin and the cycle (black, dotted line) for comparison.

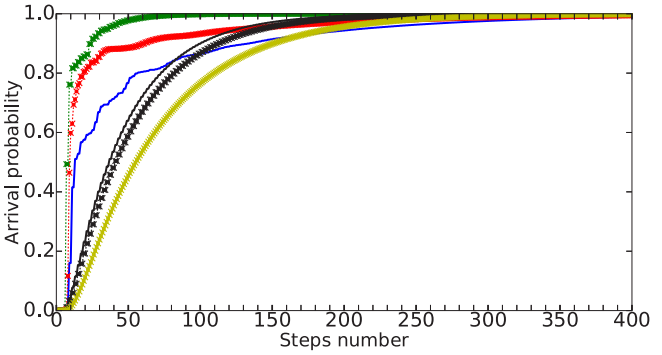


FIG. 20. A quantum walk of 400 steps on loops of zigzag (green) and armchair (red) carbon nanotube with diameters of 6 (×), 10 (dashes), and 14 (circles), and length corresponding to eight levels. Cycle $C_{14}$ (blue) shown for comparison. Corresponding classical random walks shown in black (zigzag) and yellow (armchair); classical random walk on $C_{14}$ (black, solid line).

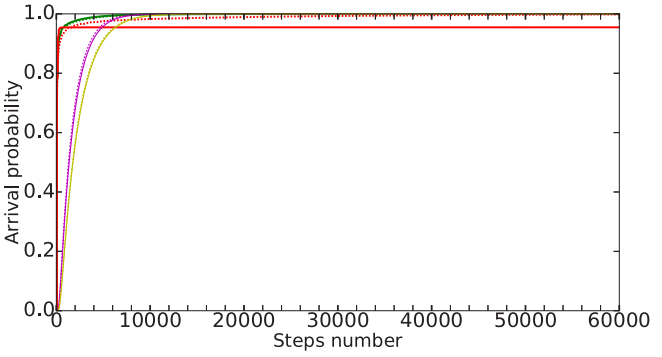


FIG. 21. A quantum walk of 60 000 steps on capped carbon nanotubes zigzag (green, solid line), armchair (red, solid line), compared with nanotube loops (dashed line), and corresponding classical random walks for zigzag (pink) and armchair (yellow), to show the long-time behavior.

as far as we can determine this from numerical studies. As Fig. 17 shows, this always happens for the cycle without a "wait" state. Furthermore, if we do not measure, we see that the classical walk converges to a constant probability to be found on the marked site, while the quantum probability continues to fluctuate for all time.

On the other hand, Fig. 18 shows that on the cycle, convergence to unity does not occur for the $F_3$ coin which includes a wait state, although it does for some others which include a wait state. This parallels some of the behavior for $C_{60}$ starting on a single site, with a single marked site. As illustrated in Fig. 19, the arrival probability converges to unity for coins without wait states, but does not for coins which do have them. We see similar behavior for the nanotube loop arrival probability depicted in Fig. 20, which depicts the results for a nanotube loop using a $G_3$ coin, and for which arrival probabilities all approach unity. However, as Fig. 21 illustrates, this is not true for all cases of capped nanotubes, in particular this probability does not approach unity for the capped armchair nanotube. It is also interesting to note that for the uncapped version of the armchair nanotube, the arrival probability does approach unity, but it does so much slower than either the zigzag nanotube or the cycle. This very slow arrival warrants future study.


[1] Julia Kempe, Discrete quantum walks hit exponentially faster, in *Approximation, Randomization, and Combinatorial Optimization.. Algorithms and Techniques*, edited by S. Arora, K. Jansen, J. D. P. Rolim, and A. Sahai, Lecture Notes in Computer Science, Vol. 2764 (Springer, Berlin, Heidelberg, 2003), pp. 354–369.

[2] Julia Kempe, Quantum random walks hit exponentially faster, Prob. Theor. Rel. Fields **133**, 215 (2005).

[3] Andrew M. Childs, Richard Cleve, Enrico Deotto, Edward Farhi, Sam Gutmann, and Daniel A. Spielman, Exponential algorithmic speedup by a quantum walk, in *Proceedings of the 35th Annual ACM STOC* (ACM, New York, 2003), pp. 59–68.

[4] S. Bose, Quantum Communication through an Unmodulated Spin Chain, Phys. Rev. Lett. **91**, 207901 (2003).

[5] A. Kay, A review of perfect state transfer and its applications as a constructive tool, Int. J. Quantum Inf. **8**, 641 (2010).

[6] A. Kay, The basics of perfect communication through quantum networks, Phys. Rev. A **84**, 022337 (2011).

[7] P. W. Anderson, Absence of diffusion in certain random lattices, Phys. Rev. **109**, 1492 (1958).

[8] J. P. Keating, N. Linden, J. C. F. Matthews, and A. Winter, Localization and its consequences for quantum walk algorithms and quantum communication, Phys. Rev. A **76**, 012315 (2007).

[9] Hari Krovi and Todd A. Brun, Hitting time for quantum walks on the hypercube, Phys. Rev. A **73**, 032341 (2006).

[10] Hari Krovi and Todd A. Brun, Quantum walks with infinite hitting times, Phys. Rev. A **74**, 042334 (2006).

[11] Hari Krovi and Todd A. Brun, Quantum walks on quotient graphs, Phys. Rev. A **75**, 062332 (2007).

[12] K. S. Novoselov *et al.*, Electric field effect in atomically thin carbon films, Science **306**, 666 (2004).

[13] K. S. Novoselov *et al.*, Two-dimensional gas of massless dirac fermions in graphene, Nature (London) **438**, 197 (2005).

[14] C. T. White and T. N. Todorov, Carbon nanotubes as long ballistic conductors, Lett. Nat. **393**, 240 (1998).

[15] J. W. Mintmire, B. I. Dunlap, and C. T. White, Are Fullerene Tubules Metallic? Phys. Rev. Lett. **68**, 631 (1992).

[16] N. Hamada, S.-i. Sawada, and A. Oshiyama, New One-Dimensional Conductors: Graphitic Microtubules, Phys. Rev. Lett. **68**, 1579 (1992).

[17] R. Saito, M. Fujita1, G. Dresselhaus, and M. S. Dresselhaus, Electronic structure of chiral graphene tubules, Appl. Phys. Lett. **60**, 2204 (1992).

[18] Matthew Dale, Julian F. Miller, Martin A. Stepney, and Susan Trefzer, Evolving carbon nanotube reservoir computers, in *Proceedings of the 15th International Conference on Unconventional Computation and Natural Computation, UCNC 2016, Manchester, United Kingdom, July 2016*, edited by Martyn Amos and Anne Condon (Springer International, Cham, 2016), pp. 49–61.

[19] Sander J. Tans, Alwin R. M. Verschueren, and Cees Dekker, Room-temperature transistor based on a single carbon nanotube, Lett. Nat. **393**, 49 (1998).

[20] Adrian Bachtold, Peter Hadley, Takeshi Nakanishi, and Cees Dekker, Logic circuits with carbon nanotube transistors, Science **294**, 1317 (2001).

[21] Woo Jong Yu *et al.*, Adaptive logic circuits with doping-free ambipolar carbon nanotube transistors, Nano Lett. **9**, 1401 (2009).

[22] Kester Dean Clegg, Julian Francis Miller, Kieran Massey, and Mike Petty, Travelling salesman problem solved 'in materio' by evolved carbon nanotube device, in *Parallel Problem Solving from Nature–PPSN XIII: Proceedings of the 13th International Conference, Ljubljana, Slovenia, September 2014*, edited by Thomas Bartz-Beielstein, Jürgen Branke, Bogdan Filipič, and Jim Smith (Springer International, Cham, 2014), p. 692.

[23] Iain Foulger, Sven Gnutzmann, and Gregor Tanner, Quantum walks and quantum search on graphene lattices, Phys. Rev. A **91**, 062323 (2015).

[24] Changyuan Lyu, Luyan Yu, and Shengjun Wu, Localization in quantum walks on a honeycomb network, Phys. Rev. A **92**, 052305 (2015).

[25] M. A. Jafarizadeh and R. Sufiani, Investigation of continuous-time quantum walk on root lattice and honeycomb lattice, Physica A: Stat. Mech. Appl. **381**, 116 (2007).

[26] G. Abal, R. Donangelo, F. L. Marquezino, and R. Portugal, Spatial search in a honeycomb network, Math. Struct. Comput. Sci. **20**, 999 (2010).

[27] D. Aharonov, A. Ambainis, J. Kempe, and U. Vazirani, Quantum walks on graphs, in *Proceedings of the 33rd Annual ACM STOC* (ACM, New York, 2001), pp. 50–59.

[28] Christopher Moore and Alexander Russell, Quantum walks on the hypercube, in *Proceedings of the 6th International Workshop on Randomization and Approximation Techniques in Computer Science (RANDOM '02)*, edited by J. D. P. Rolim and S. Vadhan (Springer, London, 2002), pp. 164–178.

[29] Andris Ambainis, Eric Bach, Ashwin Nayak, Ashvin Vishwanath, and John Watrous, One-dimensional quantum walks, in *Proceedings of the 33rd Annual ACM STOC* (ACM, New York, 2001), p. 60.

[30] Geoffrey Grimmett, Svante Janson, and Petra Scudo, Weak limits for quantum random walks, Phys. Rev. E **69**, 026119 (2004).

[31] Alex D. Gottlieb, Svente Janson, and Petra F. Scudo, Convergence of coined quantum walks in $\mathbb{R}^d$, Inf. Dimen. Anal. Quantum Probab. Rel. Topics **8**, 129 (2005).

[32] Vivien M. Kendon and Christino Tamon, Perfect state transfer in quantum walks on graphs, J. Comp. Theor. Nanoscience **8**, 422 (2010).

[33] R. J. Angeles-Canul, R. Norton, M. Opperman, C. Paribello, M. Russell, and C. Tamon, Perfect state transfer, integral circulants and join of graphs, Quantum Inf. Comput. **10**, 325 (2010).

[34] Frederick W. Strauch, Connecting the discrete and continuous-time quantum walks, Phys. Rev. A **74**, 030301 (2006).

[35] Nandan Satapathy, Henning Hagman, Martin Zelán, Anders Kastberg, and Hema Ramachandran, Theoretical investigations of quantum walks by cold atoms in a double optical lattice, Phys. Rev. A **80**, 012302 (2009).

[36] Robin Côté, Alexander Russell, E. E. Eyler, and P. L. Gould, Quantum random walk with rydberg atoms in an optical lattice, New J. Phys. **8**, 156 (2006).

[37] Leticia Tarruell, Daniel Greif, Thomas Uehlinger, Gregor Jotzu, and Tilman Esslinger, Creating, moving and merging dirac points with a fermi gas in a tunable honeycomb lattice, Nature (London) **483**, 302 (2012).

[38] Marco Polini, Francisco Guinea, Maciej Lewenstein, Hari C. Manoharan, and Vittorio Pellegrini, Artificial honeycomb lattices for electrons, atoms and photons, Nat. Nanotechnol. **8**, 625 (2013).

[39] A continuous Hamiltonian evolution that reproduces the discrete,unitary dynamics can be obtained. See, for example, V. Kendon and B. C. Sanders, Complementarity and quantum walks, Phys. Rev. A **71**, 022307 (2005). While relevant for experimental implementations, it is not useful for this study.

[40] Małgorzata Bednarska, Andrzej Grudka, Paweł Kurzyński, Tomasz Łuczak, and Antoni Wójcik, Quantum walks on cycles, Phys. Lett. A **317**, 21 (2003).

[41] B. C. Travaglione and G. J. Milburn, Implementing the quantum random walk, Phys. Rev. A **65**, 032310 (2002).

[42] Ben Tregenna, Will Flanagan, Rik Maile, and Viv Kendon, Controlling discrete quantum walks: Coins and initial states, New J. Phys. **5**, 83 (2003).

[43] Phillip R. Dukes, Quantum state revivals in quantum walks on cycles, Results Phys. **4**, 189 (2014).

[44] G. van Rossum and F. L. Drake (eds.), Python Software Foundation, https://www.python.org/ (2006).

[45] Eric Jones, Travis Oliphant, Pearu Peterson, and others; SciPy: Open source scientific tools for Python, http://www.scipy.org/.

[46] David Ascher, Paul F. Dubois, Konrad Hinsen, James Hugunin, and Travis Oliphant, Numerical Python (1999).

[47] J. D. Hunter, Matplotlib: A 2D graphics environment; Computing In Science & Engineering, Vol. 9.

[48] Virtual NanoLab version 2016.0, QuantumWise A/S, www.quantumwise.com.

[49] Frédéric Magniez, Ashwin Nayak, Peter C. Richter, and Miklos Santha, On the hitting times of quantum versus random walks, in *Proceedings of the Twentieth Annual ACM-SIAM Symposium on Discrete Algorithms, SODA '09* (Society for Industrial and Applied Mathematics, Philadelphia, PA, 2009), pp. 86–95.